



HIF-1 α is required for development of the sympathetic nervous system

Romana Bohuslavova^{a,1}, Radka Cerychova^a, Frantisek Papousek^b, Veronika Olejnickova^{b,c}, Martin Bartos^{c,d}, Agnes Görlach^{e,f}, Frantisek Kolar^b, David Sedmera^{b,c}, Gregg L. Semenza^{g,h,1}, and Gabriela Pavlinkova^{a,1}

^aLaboratory of Molecular Pathogenetics, Institute of Biotechnology, Czech Academy of Sciences, 252 50 Vestec, Czechia; ^bInstitute of Physiology, Czech Academy of Sciences, 142 00 Prague, Czechia; ^cInstitute of Anatomy, First Faculty of Medicine, Charles University, 110 00 Prague, Czechia; ^dInstitute of Dental Medicine, First Faculty of Medicine, Charles University, 110 00 Prague, Czechia; ^eGerman Heart Centre Munich, Technical University, 80636 Munich, Germany; ^fGerman Centre for Cardiovascular Research, Partner Site Munich, Munich Heart Alliance, 80636 Munich, Germany; ^gMcKusick–Nathans Institute of Genetic Medicine, Johns Hopkins University School of Medicine, Baltimore, MD 21205; and ^hInstitute for Cell Engineering, Johns Hopkins University School of Medicine, Baltimore, MD 21205

Contributed by Gregg L. Semenza, May 1, 2019 (sent for review February 28, 2019; reviewed by Gabriel G. Haddad and Michiko Watanabe)

The molecular mechanisms regulating sympathetic innervation of the heart during embryogenesis and its importance for cardiac development and function remain to be fully elucidated. We generated mice in which conditional knockout (CKO) of the *Hif1a* gene encoding the transcription factor hypoxia-inducible factor 1 α (HIF-1 α) is mediated by an *Islet1-Cre* transgene expressed in the cardiac outflow tract, right ventricle and atrium, pharyngeal mesoderm, peripheral neurons, and hindlimbs. These *Hif1aCKO* mice demonstrate significantly decreased perinatal survival and impaired left ventricular function. The absence of HIF-1 α impaired the survival and proliferation of preganglionic and postganglionic neurons of the sympathetic system, respectively. These defects resulted in hypoplasia of the sympathetic ganglion chain and decreased sympathetic innervation of the *Hif1aCKO* heart, which was associated with decreased cardiac contractility. The number of chromaffin cells in the adrenal medulla was also decreased, indicating a broad dependence on HIF-1 α for development of the sympathetic nervous system.

sympathetic neurons | cardiac innervation | tyrosine hydroxylase | hypoxia | coronary artery branching

The heart is innervated via the autonomic nervous system, which comprises sympathetic and parasympathetic nerves that exert antagonistic effects on cardiac function. Disruption of sympathetic–parasympathetic balance in the heart is central to the pathophysiology and progression of many types of heart disease. Sympathetic innervation regulates cardiac function by increasing heart rate, conduction velocity, and myocardial contractility (1). Changes in cardiac innervation pattern and activity of the sympathetic nervous system are implicated in many cardiac pathologies, ranging from sudden infant death syndrome (2) to such common diseases of adulthood as hypertension, myocardial ischemia, cardiac arrhythmias, sudden cardiac death, and heart failure (3).

The sympathetic nervous system is composed of preganglionic neurons residing in the spinal cord (the preganglionic motor column) and postganglionic neurons forming the sympathetic ganglion chain. Postganglionic sympathetic neurons that innervate the heart are generated from trunk neural crest cells, which first migrate and form the primary sympathetic ganglia (PSG) chain near the dorsal aorta, starting at embryonic day (E) 10.5 in the mouse (4, 5). Sympathetic neuroblasts express markers associated with mature sympathetic neurons, such as tyrosine hydroxylase (TH), but still undergo proliferation (6). TH is the first enzyme in the catecholamine biosynthetic pathway that produces norepinephrine, the primary neurotransmitter released from postganglionic sympathetic neurons (7). In the second migration step, sympathetic progenitors migrate away from the dorsal aorta to form secondary sympathetic ganglia at E13.5 and undergo final differentiation into sympathetic neurons with exit from the cell cycle that peaks at E14.5 (6).

The differentiation of sympathetic neurons is induced by signaling molecules of the bone morphogenetic protein family secreted by the dorsal aorta, followed by expression of a variety of transcription factors that initiate noradrenergic and neuronal differentiation, including PHOX2A, PHOX2B, GATA2, GATA3, INSM1, HAND2, ASCL1, SOX4, and SOX11 (5, 8). Another transcription factor required for the development of sympathetic progenitors in the PSG is the LIM homeodomain protein *Islet-1* (ISL1), which acts at both early and late stages of sympathetic neurogenesis (9, 10).

Postganglionic sympathetic neurons innervating the heart are located primarily in the stellate ganglion, with minor contributions from the middle cervical and upper thoracic paravertebral sympathetic ganglia (11, 12). Cardiac sympathetic fibers originate in sympathetic ganglia, extend along large-diameter coronary vessels into the underlying myocardium, and end as sympathetic nerve terminals reaching the endocardium (13). The density of sympathetic innervation is highest in the subepicardium and central conduction system, which consists of the sinoatrial node (SAN), atrioventricular node, and bundle of His (1), and sympathetic innervation gradually decreases from the

Significance

The sympathetic nervous system plays a critical role in stimulating heart rate and contractility to increase cardiac output and thereby insure adequate tissue O₂ delivery. Altered sympathetic output contributes to cardiac pathologies, such as sudden cardiac death and heart failure. Our data provide insight into the role of the transcription factor hypoxia-inducible factor 1 α (HIF-1 α) in the development of sympathetic ganglion neurons and cardiac sympathetic innervation. We found that genetic deletion of HIF-1 α resulted in increased cell death and decreased proliferation of neuronal progenitors of the sympathetic system. These findings suggest that dysregulated HIF-1 α expression may contribute to cardiac dysfunction and disease associated with defects in the cardiac sympathetic system by affecting the function and survival of sympathetic neurons.

Author contributions: R.B., D.S., and G.P. designed research; R.B., R.C., F.P., V.O., M.B., and F.K. performed research; A.G. contributed new reagents/analytic tools; R.B., F.K., D.S., G.L.S., and G.P. analyzed data; and G.L.S. and G.P. wrote the paper.

Reviewers: G.G.H., University of California, San Diego; and M.W., Case Western Reserve University.

The authors declare no conflict of interest.

This open access article is distributed under [Creative Commons Attribution-NonCommercial-NoDerivatives License 4.0 \(CC BY-NC-ND\)](https://creativecommons.org/licenses/by-nc-nd/4.0/).

¹To whom correspondence may be addressed. Email: romana.bohuslavova@ibt.cas.cz, gsemenza@jhmi.edu, or gpavlinkova@ibt.cas.cz.

This article contains supporting information online at www.pnas.org/lookup/suppl/doi:10.1073/pnas.1903510116/-DCSupplemental.

Published online June 13, 2019.

atria to the ventricles and from the base to the apex of the heart (13).

Tissue hypoxia plays important roles in the recruitment of neural crest cells, sympathetic axon guidance, and patterning of cardiac innervation (13, 14). The master regulator of transcriptional responses to decreased O₂ availability is hypoxia-inducible factor 1 (HIF-1), a heterodimeric protein consisting of an O₂-regulated HIF-1 α subunit and a constitutively expressed HIF-1 β subunit. Germline knockout of the *Hif1a* gene results in mouse embryos with profound cardiac, vascular, and neural tube defects and developmental arrest at E8.5 (15, 16). Severe placental and vascular defects, as well as the resulting early embryonic lethality of germline *Hif1a* knockout mice, preclude an in-depth investigation of the mechanisms by which HIF-1 contributes to heart development and function.

Conditional knockout (CKO) by deletion of a floxed *Hif1a* exon 2 (*Hif1a^{loxP/loxP}*) (17) under the control of several CRE driver lines (18–20) has provided insight into the role of HIF-1 α in later stages of cardiogenesis, but no previous studies have investigated whether *Hif1a* is required for cardiac sympathetic innervation. Although TH expression is regulated by HIF-1 in certain cell types (21, 22), whether HIF-1 α is required for the development of sympathetic neurons is unclear. In this study, we generated *Hif1aCKO* mice by mating *Hif1a^{loxP/loxP}* and *Isl1-Cre* mice. Lineage studies have demonstrated *Isl1-Cre* expression in progenitors of the second heart field, pharyngeal mesoderm, hindlimbs, spinal motor neurons, cranial ganglia, dorsal root ganglia, and sympathetic chain (23, 24). Our analysis of mice with *Hif1aCKO* in ISL1-expressing cells has revealed a key role

for HIF-1 α in sympathetic innervation of the heart and development of sympathetic ganglia.

Results

Loss of HIF-1 α in ISL1⁺ Cells Leads to Neonatal Mortality and Impaired Cardiac Function. Embryonic lethality of germline *Hif1a* knockout mice by E10.5 (15, 16) precludes analysis of HIF-1 α -dependent events at later developmental stages. To address this limitation, we disrupted the HIF-1 α coding sequence in *Hif1a^{loxP/loxP}* mice (17) by expression of an *Isl1-Cre* transgene (Fig. 1A) that has been used extensively to study cardiovascular and nervous system development (24–29). To identify tissues with *Isl1*-directed expression of CRE recombinase, we crossed *Isl1-Cre* mice with *Rosa26* reporter mice, which express β -galactosidase only in the presence of CRE. Descendants of cells expressing the *Isl1-Cre* transgene were detected mainly in the heart, hindlimbs, cranial ganglia, sympathetic ganglion chain, and dorsal root ganglia at E10.5 (Fig. 1B), similar to previous reports (24). The CRE-mediated excision of *Hif1a* exon 2, which encodes the basic helix-loop-helix DNA-binding domain of HIF-1 α in *Hif1a^{loxP/loxP};Isl1-Cre* (*Hif1aCKO*) mice was very efficient, with quantitative real-time PCR (qPCR) analysis of genomic DNA revealing 77% elimination of exon 2 in the heart, whereas exon 2 copy number was not significantly different in the forebrains of control and *Hif1aCKO* mice at E10.5 (Fig. 1C).

Hif1aCKO embryos were recovered at expected Mendelian ratios at all embryonic days examined in utero (Fig. 1D and *SI Appendix, Table S1*). We analyzed cardiac development, including the outflow tract and pharyngeal arch arteries, by histological

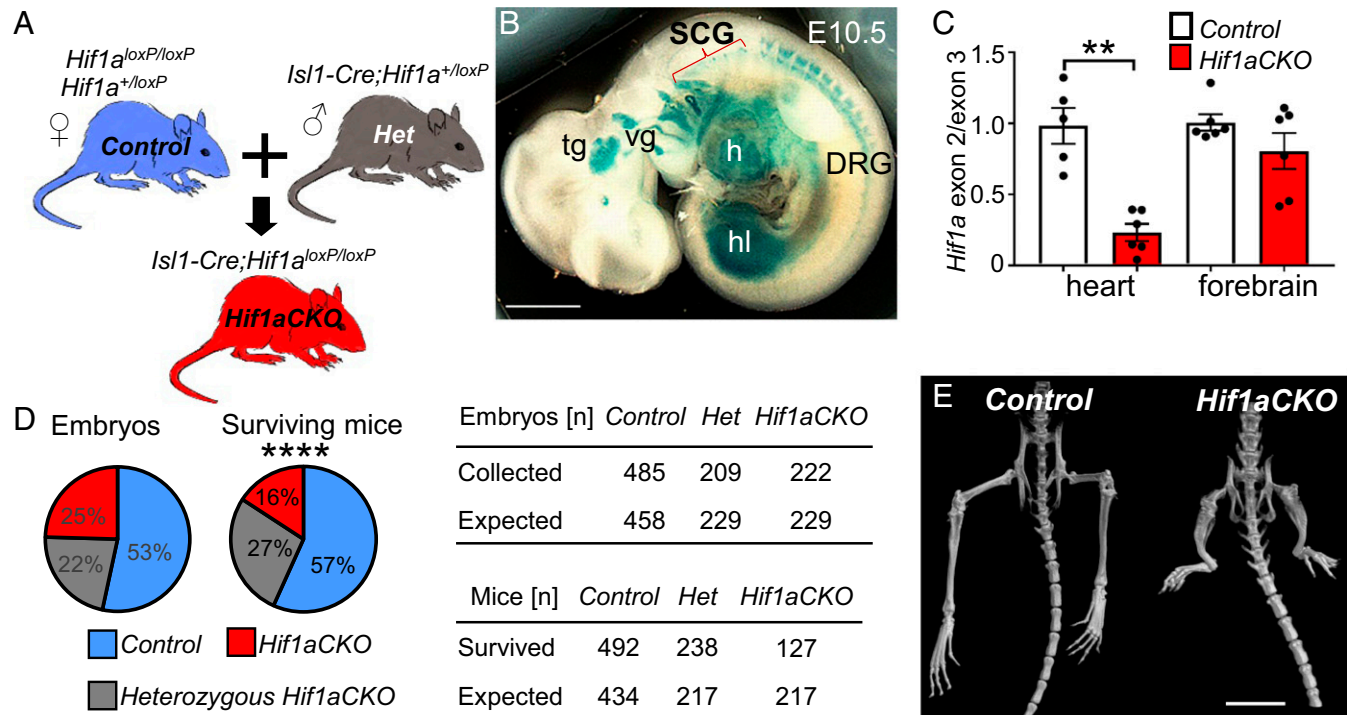


Fig. 1. Decreased neonatal survival and hindlimb malformations in *Hif1aCKO* mice. (A) The *Isl1-Cre* transgene was transmitted paternally to eliminate any potential influence of maternal HIF-1 α haploinsufficiency on the developing embryos. (B) Whole-mount X-gal staining of E10.5 *Isl1-Cre;Rosa^{26R}* embryos revealed β -galactosidase expression in the dorsal root ganglia (DRG) and sympathetic cervical ganglia (SCG), trigeminal ganglion (tg), vestibular ganglion (vg), heart (h), and hindlimb (hl). (Scale bar: 100 μ m.) (C) qPCR analysis of exon 2 (normalized to exon 3) sequences in genomic DNA isolated from heart and forebrain of *Hif1aCKO* and control embryos at E10.5. The data are presented as mean \pm SEM ($n = 6$ embryos per group). $**P < 0.01$, Student's t test. (D, Left) The genotype distribution of embryos and surviving mice. (D, Right) Observed distribution of genotypes of embryos collected between E7.5 and E17.5 according to the expected Mendelian ratio (Top). In contrast, the observed genotype distribution of surviving mice at 3 wk after birth shows a decreased number of *Hif1aCKO* mice (Bottom). $****P < 0.0001$, χ^2 test. (E) Micro-CT scan shows hindlimb malformations with reduced tibia, femur, and pelvis lengths in adult *Hif1aCKO* mice. (Scale bar: 10 mm.)

analysis of E14.5 and E15.5 embryos. *Hif1a*CKO hearts ($n = 11$) were indistinguishable from control (*Hif1a*^{+loxP} or *Hif1a*^{loxP/loxP}) hearts ($n = 7$) with no gross structural abnormalities. Thus, *Hif1a* deletion in ISL1⁺ cardiac progenitor cells did not affect overall heart development. However, *Hif1a*CKO mice had significantly increased neonatal mortality ($P < 0.0001$, χ^2 test), with 40% fewer *Hif1a*CKO mice identified at the time of genotyping (3 wk) compared with *Hif1a*^{+loxP}; *Isl1*-Cre mice (Fig. 1D). Examination of surviving adult *Hif1a*CKO mice revealed major malformations of the proximal and distal hindlimbs (Fig. 1E and *SI Appendix*, Fig. S1). Conditional inactivation of HIF-1 α during limb development using *Prx1*-Cre caused malformation of both forelimbs and hindlimbs (30).

Due to gender differences in cardiac electrophysiological properties (31), we focused our functional analyses on male mice. Since the body weight of *Hif1a*CKO mice was decreased (Fig. 2A), as was heart weight (HW) (Fig. 2B), we adjusted HW using the length of the cranial base (LCB) measured by micro-computed tomography (CT) (Fig. 2C and *SI Appendix*, Fig. S2 and Table S2). The HW of the surviving *Hif1a*CKO mice was

modestly decreased compared with age-matched controls (Fig. 2B), but the ratio of left ventricular (LV) weight to HW was unaffected (Fig. 2D). Although *Hif1a*CKO mice had no detectable structural abnormalities of the cardiac chambers or valves, analysis of adult males using echocardiography revealed significantly impaired LV function, with fractional shortening of $33.3 \pm 0.4\%$, compared with $37.0 \pm 0.9\%$ in control littermates (Fig. 2E, G, and H and *SI Appendix*, Table S3). Observed differences in heart rate were not statistically significant (Fig. 2F and *SI Appendix*, Table S3).

Impaired Sympathetic Innervation in *Hif1a*CKO Hearts. Immunohistochemical staining of TH revealed significantly impaired sympathetic innervation in the hearts of *Hif1a*CKO mice. At E14.5, TH⁺ sympathetic axons were found on the heart surface and in an area adjacent to the sinus venosus, reaching the base of the ventricles in control hearts, whereas in *Hif1a*CKO hearts, TH⁺ axons were significantly reduced in number and length and were restricted to the area of the sinus venosus (Fig. 3A). Between E14.5 and E17.5, sympathetic axons extended to and branched in the dorsal subepicardium of control hearts, whereas expansion of sympathetic innervation in the *Hif1a*CKO hearts was attenuated. In comparison with control littermates, sympathetic innervation was significantly decreased in E16.5 *Hif1a*CKO hearts (Fig. 3B). In contrast to the abundant TH⁺ neurons in control hearts (Fig. 3C), considerable variation in sympathetic innervation of *Hif1a*CKO hearts was observed, ranging from a 30% reduction to a complete absence of TH⁺ neurons (Fig. 3D). Decreased sympathetic innervation was also detected in the hearts of surviving 3-mo-old *Hif1a*CKO mice, as shown by anti-TH and anti-TUJ1 immunofluorescence (Fig. 3E–H). Consistent with the reduced innervation of *Hif1a*CKO hearts at E14.5, reverse-transcription and qPCR revealed decreased levels of mRNA encoding TH as well as nerve growth factor (NGF) (Fig. 3I), which is required for terminal sympathetic innervation of target tissues (32).

Since ISL1 is expressed in the SAN during the development of cardiac pacemaker cells (33), we investigated formation of the SAN in *Hif1a*CKO hearts. Hyperpolarization-activated nucleotidated cation channel 4 (HCN4) is a well-established marker for slow-conducting components of the cardiac conduction system with pacemaker potential (34). At E16.5, formation of the SAN was comparable between genotypes, although innervation in the proximity of the SAN was reduced, thinner, and more disorganized in *Hif1a*CKO hearts compared with control hearts (Fig. 3J and K).

The gap junction alpha 1 (GJA1) protein, also known as connexin 43 (CX43), plays a key role in myocardial conduction, and decreased CX43 expression is associated with decreased conduction properties in a heart failure model (35). Furthermore, HIF-1 binds directly to the *GJA1* gene and activates its transcription in hypoxic melanoma cells (36). Immunohistochemistry (Fig. 4A, Upper) and image analysis (Fig. 4A, Lower) revealed significantly decreased CX43 protein levels in the compact myocardium of the LV in *Hif1a*CKO hearts compared with controls (Fig. 4B).

Aberrant Coronary Artery Architecture in *Hif1a*CKO Hearts. The physical proximity and similar branching pattern of the coronary vasculature and peripheral nerves imply coordinated development of these networks. Since sympathetic innervation was impaired in *Hif1a*CKO hearts, we investigated coronary vascular architecture using Microfil injection (Flow Tech) and micro-CT. Quantification of the branching pattern (i.e., frequency and distance of identifiable branches from the left coronary artery) did not reveal any significant differences between control and *Hif1a*CKO adult mice (*SI Appendix*, Table S4). As described previously (37), the most common coronary architecture was the presence of two independent coronary arteries originating from the left and right aortic sinuses, with the septal artery originating from the right coronary artery (Fig. 5A and B). However, in

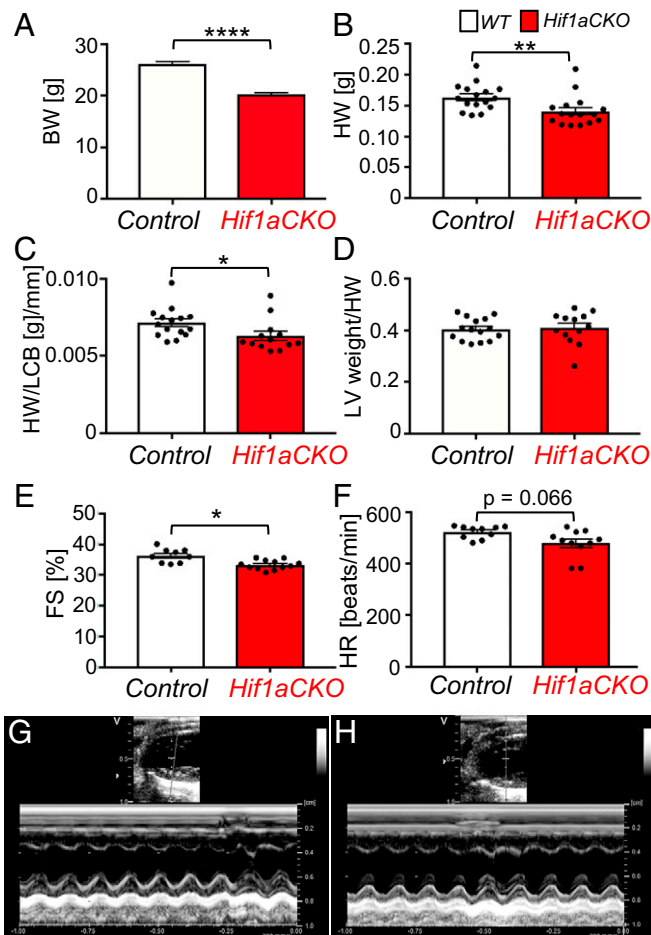


Fig. 2. Impaired LV function in *Hif1a*CKO mice. (A) Body weight (BW) was decreased in adult *Hif1a*CKO mice ($n = 37$) compared with controls ($n = 40$). (B and C) Both HW and HW relative to the LCB (HW/LCB) were decreased in *Hif1a*CKO mice ($n = 13$) compared with controls ($n = 15$). (D) The ratio of LV weight to HW (LV/HW) was not significantly different between genotypes. (E and F) Echocardiographic analyses of adult (3-mo-old) males revealed significantly decreased fractional shortening (FS) but no significant difference in heart rate (HR) in *Hif1a*CKO mice ($n = 12$) compared with control mice ($n = 10$). (G and H) Representative M-mode echocardiography (long-axis view of LV) in control (G) and *Hif1a*CKO (H) mice. All numerical data are presented as mean \pm SEM. * $P < 0.05$, ** $P < 0.01$, **** $P < 0.0001$, Student's *t* test.

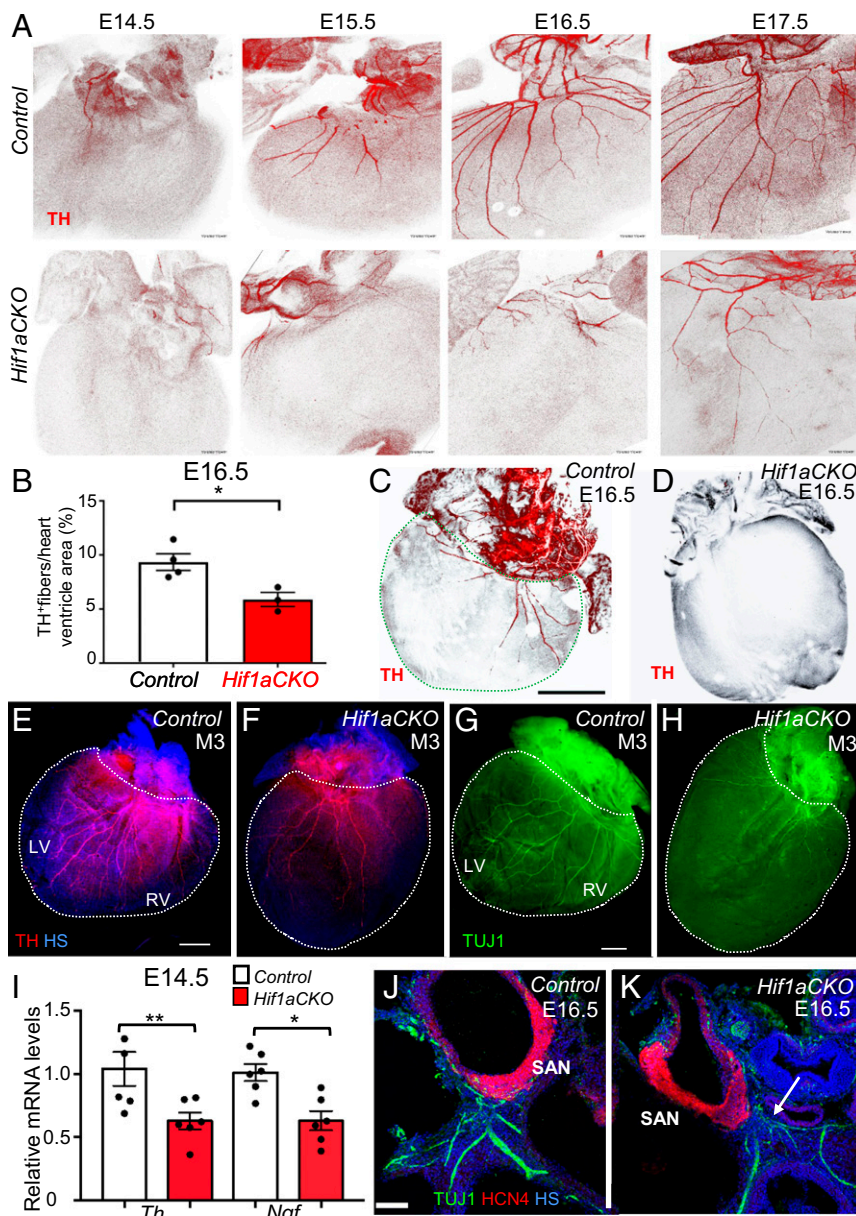


Fig. 3. Impaired sympathetic innervation of *Hif1aCKO* hearts. (A) Immunohistochemical staining of TH in posterior view of hearts from control (Upper) and *Hif1aCKO* (Lower) littermate embryos between E14.5 and E17.5. (B) Quantification of TH⁺ fibers per ventricle area in E16.5 control and *Hif1aCKO* hearts ($n = 4$ each). * $P < 0.05$, Student's t test. (C and D) Posterior view of E16.5 control heart (C) and *Hif1aCKO* heart with no detectable TH⁺ fibers (D). In C, the dashed green line demarcates the ventricular area of the heart. (Scale bar: 500 μm .) (E–H) Sympathetic innervation of hearts from 3-mo-old male mice (M3) was analyzed by anti-TH (E and F) and anti-TUJ1 (G and H) immunohistochemistry. The posterior view is shown, and dotted lines encompass the left ventricle (LV) and right ventricle (RV) of the heart. (Scale bar: 1 mm.) (I) Relative *Th* and *Ngf* mRNA levels were measured by reverse-transcription and qPCR, using mRNA extracted from the whole heart at E14.5, when the sympathetic neurons reach the heart and start to innervate the ventricles ($n = 8$ hearts per genotype). * $P < 0.05$, ** $P < 0.01$, Student's t test. (J and K) Expression of HCN4, a marker for the cardiac conduction system, in E16.5 heart sections. HCN4⁺ area of the SAN in the *Hif1aCKO* embryo is comparable to that in the control embryo at E16.5, but TUJ1-labeled nerve fibers in proximity of the SAN are reduced, thinner, and more disorganized in the *Hif1aCKO* (arrow) compared with control heart. (Scale bar: 100 μm .) HS, Hoechst stain. All numerical data are presented as mean \pm SEM.

2 out of 13 *Hif1aCKO* hearts, we detected a major anomaly in which a single coronary artery arose from the right aortic sinus, from which the left coronary and septal arteries then originated (Fig. 5 C and D). This type of coronary artery anomaly, which was observed in none of 15 control hearts, is considered a pathological malformation in humans (37).

HIF-1 α Is Required for Development of Sympathetic Ganglia. Based on our finding of compromised sympathetic innervation of the

heart in *Hif1aCKO* mice, we assessed the development of the sympathetic nervous system more broadly (Fig. 6). ISL1 expression is initiated in the developing sympathetic progenitors at E9.5 and is maintained in sympathetic ganglia until E16.5 (9). ISL1 is also expressed in developing preganglionic motor neurons of the ventral spinal cord (38). We first analyzed the expression of ISL1 and TH, the marker of sympathetic lineage cells, at E10.5. TH expression was reduced in preganglionic motor neurons and their axons within the thoracic spinal cord of *Hif1aCKO* mice compared with control

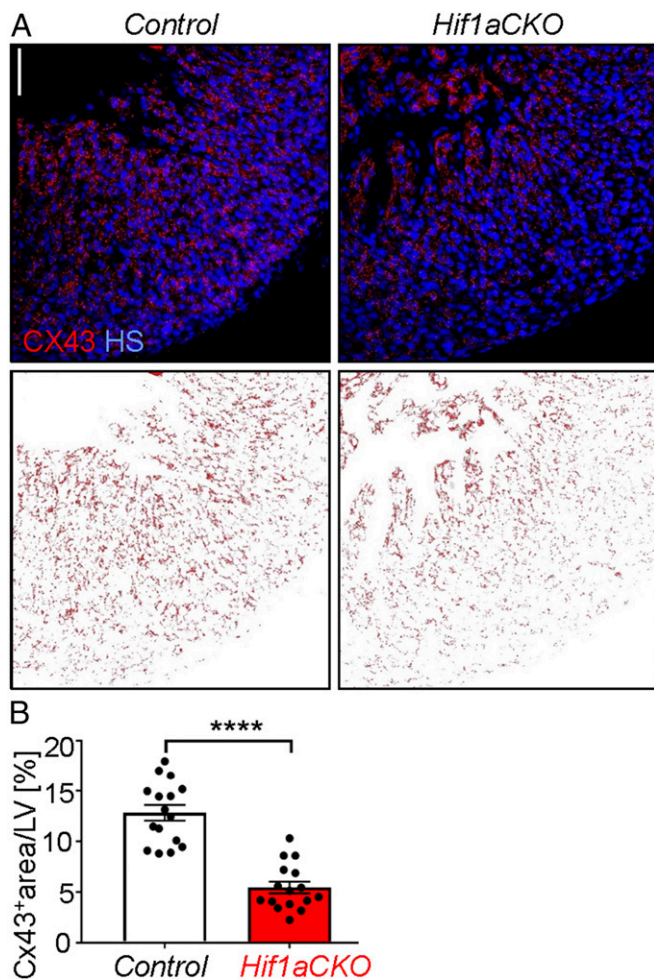


Fig. 4. Decreased connexin 43 expression in *Hif1aCKO* hearts at E16.5. (A) CX43 immunohistochemistry was performed (Upper), and the CX43⁺ area was captured using ImageJ (Lower). (Scale bar: 50 μ m.) (B) CX43 staining was quantified using ImageJ, and the CX43⁺ area was expressed as percentage of total cross-sectional area of compact myocardium of LV in control and *Hif1aCKO* littermates ($n = 3$ embryos per genotype and 4–6 fields per LV). **** $P < 0.0001$, Student's t test. The data are presented as mean \pm SEM.

littermates (Fig. 6 A–D). The TH⁺ domain was significantly decreased in motor neuron columns of *Hif1aCKO* embryos (Fig. 6K). TH and ISL1 expression appeared to be decreased in neurons of developing PSG of *Hif1aCKO* mice compared with controls (Fig. 6 E and F). At E11.5, HIF-1 α expression was almost completely absent in thoracic motor columns of *Hif1aCKO* embryos compared with control littermates (Fig. 6 G and H).

To determine whether the impaired development of sympathetic ganglia was due to altered proliferation or survival, we first performed immunostaining for cleaved caspase 3, which revealed significantly increased apoptosis of preganglionic neurons in motor columns of E11.5 *Hif1aCKO* embryos (Fig. 6 I, J, and K). The ISL1⁺ domain was significantly decreased in *Hif1aCKO* motor columns compared with controls (Fig. 6M). Since developing preganglionic neurons and postganglionic sympathetic neurons interact extensively (39), increased death of preganglionic neurons may influence the formation of sympathetic ganglia. In contrast to increased apoptosis of neurons in the neural tube, no caspase 3-positive cells were observed in the PSG of *Hif1aCKO* or control embryos at E11.5 (Fig. 6 P and Q).

However, Ki67 immunostaining revealed significantly attenuated proliferation of sympathetic neurons in the developing ganglia in *Hif1aCKO* embryos at E11.5 (Fig. 6 R–T), when most sympathetic neurons have reentered the cell cycle until their terminal differentiation (6). Taken together, these data suggest that HIF-1 α is required for proliferation of progenitors of the sympathetic ganglia and for survival of preganglionic neurons in the developing thoracic spinal cord. Consistent with these changes, axon projections in the cervical and upper thoracic area were diminished in *Hif1aCKO* embryos compared with control embryos at E11.5 (Fig. 7). Axonal bundles of sympathetic neurons also appeared thinner in *Hif1aCKO* embryos (Fig. 7 C and D).

We next investigated formation of the secondary sympathetic ganglia. Hypoplasia of PSG was accompanied by decreased overall size of the secondary sympathetic chain ganglia in *Hif1aCKO* embryos. The superior cervical ganglia, stellate ganglia, and thoracic sympathetic chain ganglia of *Hif1aCKO* embryos were noticeably smaller than those of littermate controls at E14.5 as visualized by TH immunostaining (Fig. 8 A and B). We focused our analyses on the stellate ganglia, where the overwhelming majority of cardiac nerve fibers originate (12). To assess the functional state of neurons in the stellate ganglia, we evaluated the expression of neuronal nuclear antigen (NeuN), a differentiation marker of mature postmitotic neurons. The number of NeuN⁺ neurons in the stellate ganglia of *Hif1aCKO* embryos was significantly decreased (Fig. 8 C–F). Using NeuN whole-mount staining, we determined that *Hif1aCKO* ganglia were 34% smaller compared with those of littermate controls at E14.5 (Fig. 8F and SI Appendix, Fig. S3). At E14.5, strong nuclear HIF-1 α was detected in neurons of the stellate ganglia in control embryos (Fig. 8G), whereas HIF-1 α expression was reduced and localized to the

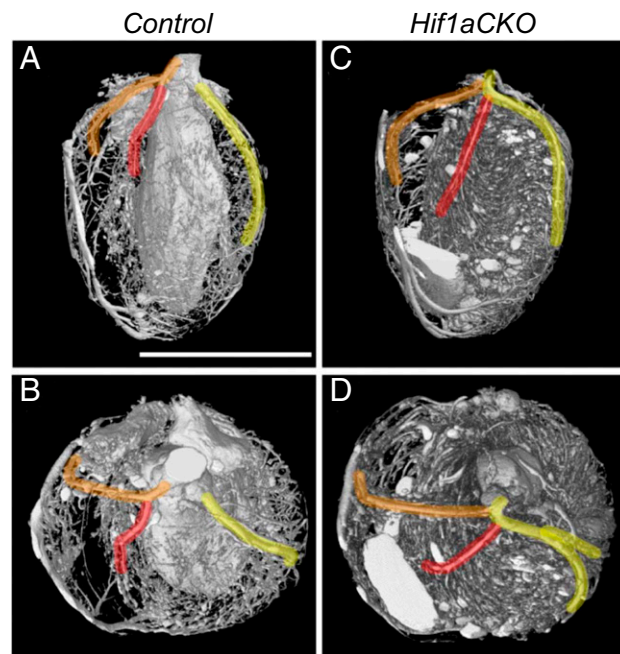


Fig. 5. Main coronary artery anomalies in *Hif1aCKO* hearts. Micro-CT visualization of coronary artery branching patterns in 2-mo-old control (A and B) and *Hif1aCKO* (C and D) mice. Anterior aspect (A and C) and top view (B and D) are shown. Arteries are highlighted from their origin: right coronary artery (RCA; orange), left coronary artery (LCA; yellow), and septal artery (SA; red). The classic arrangement with two independent coronary arteries, the RCA and LCA, arising separately from the aorta and the SA arising from the RCA was observed in 15 out of 15 control hearts (A and B). An anomalous single coronary artery arising from the aorta with subsequent division of the RCA, SA, and LCA was observed in 2 out of 13 *Hif1aCKO* hearts (C and D). (Scale bar: 5 mm.)

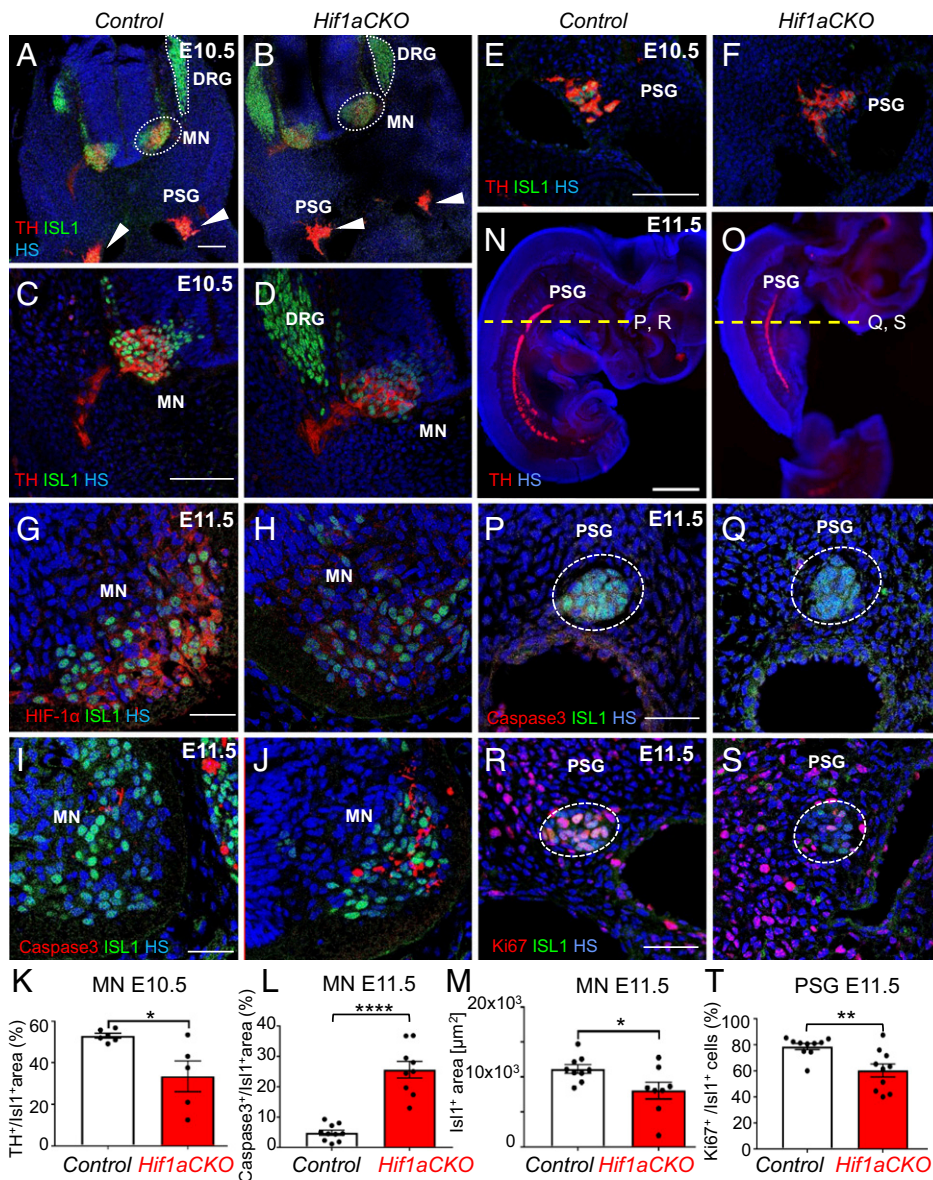


Fig. 6. Abnormal development of sympathetic neurons in *Hif1aCKO* embryos. (A and B) Cross-section images of E10.5 embryos showing decreased expression of TH (red) in developing neurons of the sympathetic system in *Hif1aCKO* embryos compared with control embryos. ISL1⁺ neurons (green) were detected in the dorsal root ganglia (DRG), in developing motor neuron populations (including preganglionic motor columns of the sympathetic system) within the ventral neural tube (MN), and in forming PSG (arrowheads). TH expression was detected in the MN, sympathetic axons, and PSG neurons. HS is shown in blue. (C–F) Higher magnification images show TH expression in the MN (C and D) and PSG (E and F). (G and H) HIF-1 α expression (red) was decreased in the MN of *Hif1aCKO* embryos compared with control embryos. (I, J, L, and M) Cleaved caspase-3 immunostaining shows significantly increased apoptosis and decreased ISL1⁺ area in the MN of *Hif1aCKO* embryos at E11.5 ($n = 5$ embryos per genotype and 2 ganglia per embryo). **** $P < 0.0001$, Mann–Whitney U test; * $P < 0.05$, Student’s t test. (K) Quantification of TH⁺ area as a percentage of the total ISL1⁺ area in the MN ($n = 3$ embryos per genotype and two sections per embryo). * $P < 0.05$, Student’s t test. (N and O) Sagittal sections of E11.5 embryos were analyzed by TH immunostaining to identify the PSG. The dotted yellow line indicates the plane of cross-sectioning for the images shown in P–S. (P and Q) Cross-sections of E11.5 embryos show no apoptotic cells in PSG neurons of control or *Hif1aCKO* embryos ($n = 5$ embryos per genotype analyzed). (R and S) Immunostaining for proliferating cell nuclear antigen Ki67 (red) in PSG neurons. (T) Quantification of proliferating neurons in PSG of control and *Hif1aCKO* embryos ($n = 5$ embryos per genotype and 2 ganglia per embryo). ** $P < 0.01$, Student’s t test. (Scale bars: 100 μm for A–F, 50 μm for G–J and P–S, and 1,000 μm for N and O.) All numerical data are presented as mean \pm SEM.

cytoplasm of TH⁺ neurons in *Hif1aCKO* embryos (arrowheads in Fig. 8H). The cross-sectional area of the stellate ganglia (dotted ovals in Fig. 8G and H) was decreased in *Hif1aCKO* embryos. Thus, the loss of HIF-1 α expression and differentiated neurons in sympathetic chain ganglia correlates with the attenuated sympathetic innervation of *Hif1aCKO* hearts and impaired development of secondary sympathetic ganglia at E14.5.

Development of Adrenal Chromaffin Cells Is Impaired in *Hif1aCKO* Embryos. Since sympathetic neurons and neuroendocrine chromaffin cells in the adrenal medulla derive from a common catecholaminergic sympathoadrenal progenitor (9), we analyzed the development of adrenal chromaffin cells in *Hif1aCKO* embryos. We first analyzed TH expression in the adrenal medulla at E17.5, and found that TH expression in the adrenal medulla of *Hif1aCKO* embryos was only 55% of that of control littermates

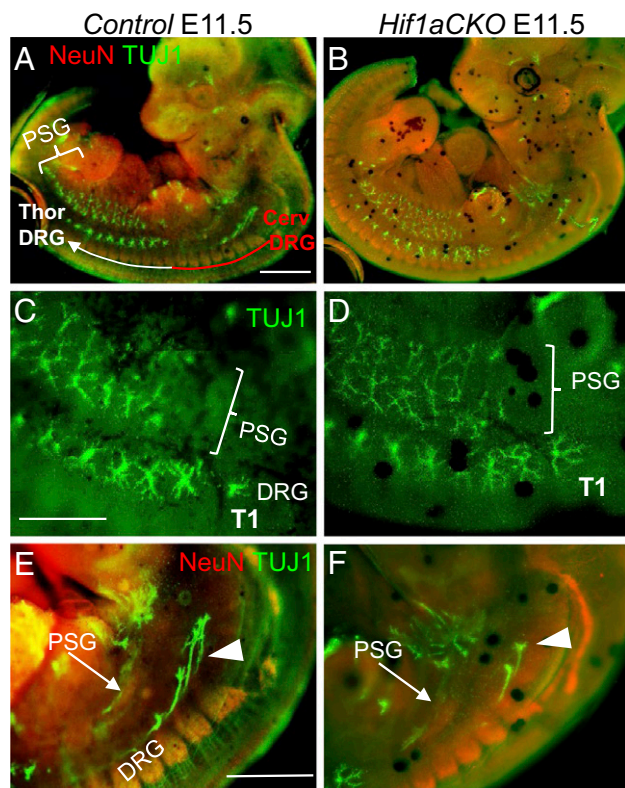


Fig. 7. HIF-1 α is required for normal axon growth. (A and B) Whole-mount immunostaining of nerve fibers with anti-TUJ1 (green) shows decreased innervation in the cervical area of the DRG and developing PSG in *Hif1aCKO* embryos compared with control embryos at E11.5. Neurons are labeled with anti-NeuN (red). The cervical (red line) and thoracic (white line) DRG are indicated in A. (C–F) Higher-magnification images of the upper thoracic region show thinner axonal bundles of neurons in PSG (arrows in E and F) and decreased numbers of DRG axons (arrowheads in E and F) in *Hif1aCKO* embryos compared with control embryos. Thoracic T1 vertebra are indicated in C and D. (Scale bars: 1,000 μm for A, B, E, and F; 500 μm for C and D)

(Fig. 9 A–C). We next analyzed expression of chromogranin A, a secretory protein located in chromaffin vesicles that is costored and coreleased with catecholamines, in the adrenal medulla. The chromogranin A expression domain in the adrenal gland was also decreased in *Hif1aCKO* compared with control littermates (Fig. 9 D–F). These findings show that HIF-1 α deficiency affects the development of chromaffin cells as well as sympathetic neurons.

Discussion

In this study, we generated conditional deletion of the *Hif1a* gene to bypass the early embryonic lethality associated with germline *Hif1a* knockout (15, 16). We found that mice selectively lacking HIF-1 α in ISL1⁺ cells have a profound deficit in sympathetic innervation of the heart and impaired development of sympathetic ganglia and chromaffin cells. Thus, HIF-1 α is essential for the development of neuronal and endocrine sympathoadrenal lineage derivatives.

HIF-1 α is required for physiological responses to hypoxia and plays critical roles in the pathophysiology of cancer, cardiovascular disease, and other common causes of mortality (40, 41). During development, HIF-1 α is required for circulatory system development and O₂ homeostasis (15, 40, 42). Mice lacking *Hif1a* expression die at midgestation due to profound cardiovascular and neural tube defects (15, 16). We previously reported that global *Hif1a* haploinsufficiency in combination with an

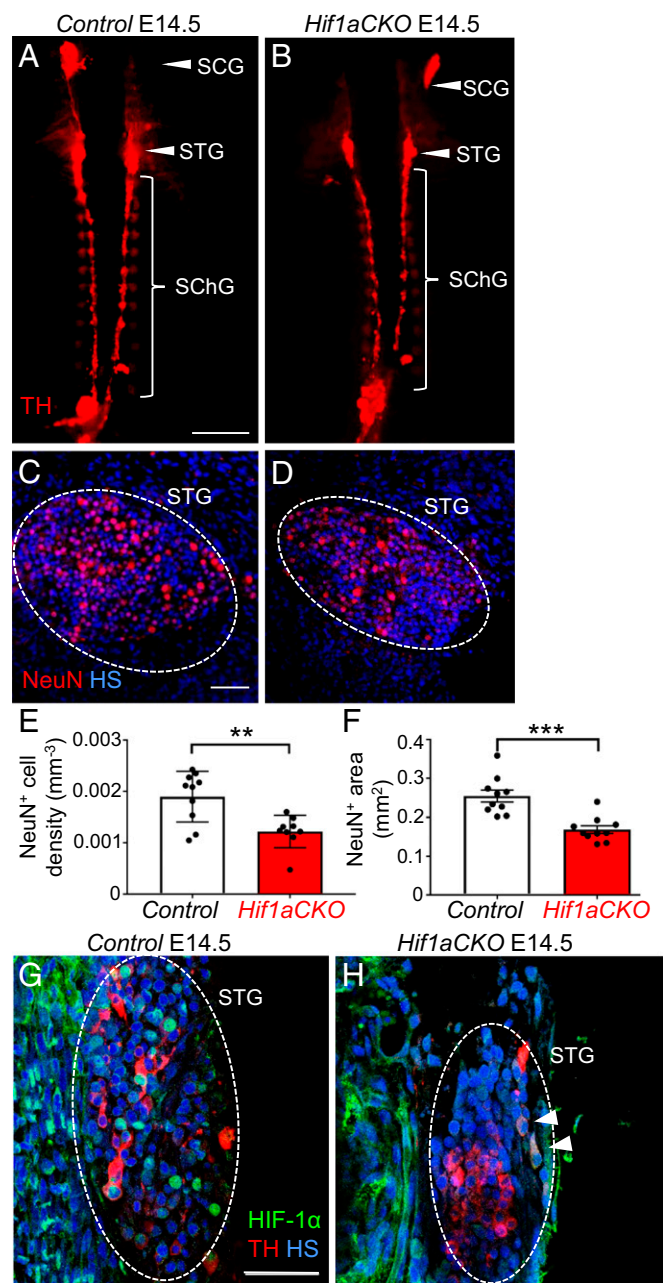


Fig. 8. The growth and maturation of secondary sympathetic ganglia are impaired in E14.5 *Hif1aCKO* embryos. (A and B) Whole-mount TH immunostaining was performed to detect the secondary chain of sympathetic ganglia, which are smaller in *Hif1aCKO* mice compared with control littermates. Arrowheads indicate the superior cervical (SCG) and stellate (STG) ganglia; bracket indicates the thoracic chain of sympathetic ganglia (SchG). (Scale bar: 1,000 μm .) (C and D) Immunostaining for NeuN (a marker for differentiated neurons; red) shows reduced neuronal density in the STG of *Hif1aCKO* compared with control embryos ($n = 5$ embryos per genotype and 2 ganglia per embryo). $^{**}P < 0.01$, Student's *t* test. (Scale bar: 50 μm .) (E and F) Morphometry of sympathetic ganglia (the STG and three upper ganglia of the thoracic sympathetic chain) by whole-mount NeuN immunostaining of the spinal cord ($n = 5$ embryos per genotype, left and right sympathetic chain ganglia per embryo). $^{***}P < 0.0005$, Student's *t* test. (G and H) Coronal sections of embryos immunolabeled with anti-TH (red) and anti-HIF-1 α (green) show a smaller STG area (dotted oval) and lower HIF-1 α expression in *Hif1aCKO* embryos. Strong HIF-1 α expression was detected in nuclei of TH⁺ neurons in control embryos (G) but only in the cytoplasm of a few TH⁺ neurons in *Hif1aCKO* embryos (H, arrowheads). (Scale bar: 50 μm .) All numerical data are presented as mean \pm SEM.

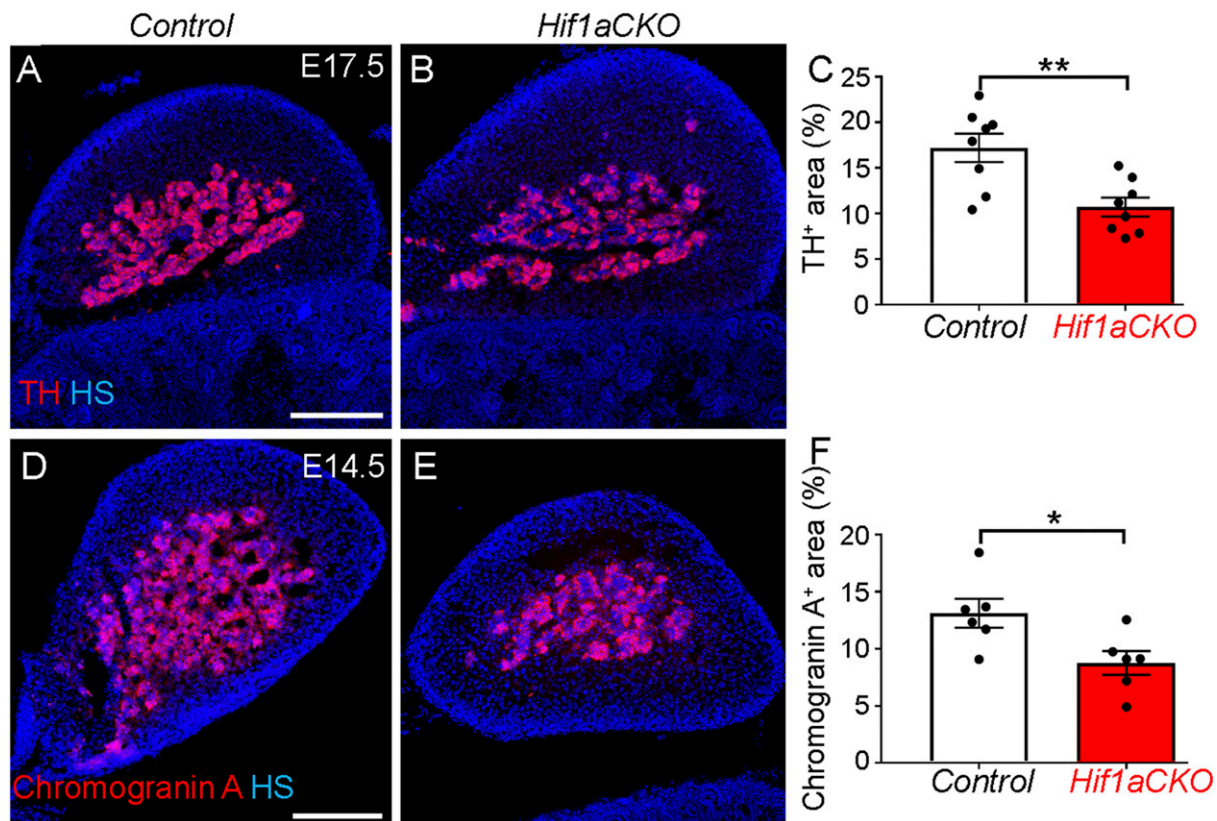


Fig. 9. Decreased number of adrenal chromaffin cells in *Hif1aCKO* embryos. (A and B) Cross-sections through the adrenal glands of *Hif1aCKO* and control embryos at E17.5 were stained with anti-TH antibody (red). (C) TH⁺ area was quantified using ImageJ software and expressed as percentage of total adrenal gland area ($n = 4$ embryos per genotype and two sections per embryo). $**P < 0.005$, Student's *t* test. (D and E) Chromogranin A expression in cross-sections of the adrenal glands of control and *Hif1aCKO* E14.5 embryos was detected by immunostaining. (F) Chromogranin A⁺ area was quantified using ImageJ and expressed as a percentage of the total adrenal gland area ($n = 3$ embryos per genotype and two sections per embryo). $*P < 0.05$, Student's *t* test. (Scale bar: 200 μm .) All numerical data are presented as mean \pm SEM.

adverse diabetic environment in utero is associated with an increased incidence of congenital cardiac defects and impaired cardiac function (43, 44). In the present study, we used an *Isl1-Cre* transgene to generate selective HIF-1 α deficiency. ISL1 is expressed in progenitors of the cardiac outflow tract, right ventricle and atria (23), hindlimbs, and all peripheral neurons (45). ISL1 regulates both early and late development of the sympathetic nervous system, including axon growth as well as neuron proliferation and maturation (10).

Isl1-Cre-mediated excision of *Hif1a* exon 2 did not affect heart development at a gross morphological level, as the chambers and outflow tract were comparable between control and *Hif1aCKO* embryos. Thus, the disruption of *Hif1a* in ISL1⁺ cardiac progenitor cells did not affect cardiac morphogenesis. This conclusion is consistent with the recent finding that ISL1⁺ cardiac progenitor cells proliferate in a normoxic niche with low HIF-1 α expression (46). Conversely, HIF-1 α forms a repressor complex to silence *Isl1* expression under pathological hypoxia, leading to congenital cardiac defects (46).

In attempting to understand how HIF-1 α loss of function in ISL1⁺ cells influences neonatal survival and cardiac function of *Hif1aCKO* mice, we uncovered an essential role for HIF-1 α in the development of cardiac sympathetic neurons. We observed significantly impaired sympathetic innervation of *Hif1aCKO* hearts compared with littermate control hearts at E14.5. Expression of the *Th* gene, a direct target of HIF-1 (21), was decreased in the heart at E14.5, when sympathetic nerve terminals reach the heart and begin to innervate the ventricles. The expression of mRNA encoding NGF, which is required for cardiac

sympathetic innervation and axon growth (32, 47, 48), was also reduced in E14.5 *Hif1aCKO* hearts. We cannot rule out the possibility that these changes in gene expression represent the consequence, rather than the cause, of decreased sympathetic innervation or reflect an indirect effect of HIF-1 α loss of function. We also cannot exclude the possibility that impaired production of neurotrophic factors by cardiac myocytes might contribute to impaired cardiac innervation. However, the impaired development of sympathetic chain ganglia suggests direct effects of HIF-1 α deficiency on sympathetic neurons.

In addition to the impaired sympathetic innervation, CX43 expression was significantly decreased in *Hif1aCKO* hearts. CX43 is an integral membrane protein and the major gap junction protein that contributes to the electrical coupling of ventricular cardiomyocytes (49). A single nucleotide polymorphism in the *GJA1* gene encoding CX43 is associated with arrhythmias and sudden cardiac death (50). CX43 is a key mediator of cardiomyocyte protection during hypoxia (51), and CX43 expression is directly regulated by HIF-1 in melanoma cells (36). Decreased CX43 expression in the LV of *Hif1aCKO* mice may have contributed to the impaired contractility detected on echocardiography and may have increased the risk of arrhythmias and sudden death. *Isl1* expression has been documented in cardiac pacemaker cells (33, 52), providing another potential mechanism for arrhythmias in *Hif1aCKO* mice.

It is interesting that increased neonatal mortality was reported in mice with germline deletion of *Th*, and that, as in the case of *Hif1aCKO* mice, no pathological abnormalities were found in *Th*^{-/-} mice that could definitively establish the primary cause of

death (53). It is possible that the neonatal mortality of *Hif1aCKO* mice is due to reduced catecholamine production or defective sympathetic innervation of other tissues, such as the lungs, because a catecholamine surge at birth is critical to maintain euglycemia (53) and trigger the pulmonary fluid absorption necessary to increase lung compliance and pulmonary function (54). A number of additional mechanisms underlying sudden infant death syndrome have been proposed, including inborn errors of metabolism, respiratory dysfunction, cardiorespiratory instability, and cardiac arrhythmias (55). Finally, the hindlimb defects of *Hif1aCKO* mice might impair suckling and thereby contribute to neonatal mortality, but conditional inactivation of *Hif1a* in the limb bud mesenchyme using *Pxl-Cre* resulted in severe forelimb and hindlimb shortening without any effect on neonatal survival (30).

Within the central nervous system, blood vessels modulate neurogenesis and neuronal migration (56), and neurons reciprocally regulate angiogenesis by expressing angiogenic factors (57). Similarly, the development and function of peripheral innervation and vasculature in the heart depend on precise communication between the nervous and vascular systems (13). Based on our finding of impaired sympathetic innervation, as well as on genetic and toxicologic data linking HIF-1 to coronary development (58, 59), we analyzed the arrangement of coronary arteries. Notably, in 15% of *Hif1aCKO* hearts, we observed a single coronary artery (from the right aortic sinus), which is considered a major anomaly in human pathology associated with myocardial ischemia (37). We interpreted this as a defect in remodeling of the periaortic plexus, from which two coronary arteries normally form, one penetrating to the left aortic sinus and the other to the right aortic sinus. Major coronary anomalies could be the cause of death in a proportion of the *Hif1aCKO* mice. Further studies are needed to identify the major defects in cardiac vascularization or innervation (e.g., Fig. 3D) that are found in late-stage *Hif1aCKO* fetuses more frequently than in surviving *Hif1aCKO* neonates and thus are likely to contribute to neonatal mortality.

Multiple transcription factors drive the development of sympathetic neurons (4, 5), and our results demonstrate that HIF-1 α is involved in this process. We found that HIF-1 α loss of function resulted in significantly decreased TH expression and increased cell death in neurons of the preganglionic motor columns. Furthermore, reduced proliferation of sympathetic progenitors in the PSG impaired the development of sympathetic chain ganglia and sympathetic innervation of the heart, demonstrating a continued requirement for HIF-1 α at later stages of sympathetic neuron differentiation and maturation. As a master regulator of responses to hypoxia, HIF-1 signaling directly or indirectly targets hundreds of genes (40). HIF-1 has been shown in different cell types to regulate genes involved in a regulatory network of early sympathetic neuron development, for example, bone morphogenetic protein signaling (60), *Hand1* and *Hand2* (16), *Th* (21), and *Sox4* (61). In addition, HIF-1 is an important regulator of a key angiogenic factor, vascular endothelial growth factor (VEGF), which is essential for the regulation of axon growth (62). Nerve-derived VEGF is required for arterial differentiation (63), and decreased VEGF levels cause neuron degeneration (64).

The present study has uncovered a requirement for HIF-1 α in cardiac sympathetic neurogenesis, whereas germline knockout of the *Phd3* gene causes abnormal adrenal and sympathetic nervous system development due to HIF-2 α overexpression (65). HIF-1 α is required for sympathetic nervous system activation mediated by the carotid body, and its action is opposed by HIF-2 α (66). Our findings raise the intriguing possibility that in addition to its critical role in the development of sympathetic neurons, HIF-1 α may play a role in various sympathetic abnor-

malities underlying cardiac pathologies, such as sudden cardiac death and heart failure.

Materials and Methods

Expanded descriptions of our animal models and methodology are provided [SI Appendix, Materials and Methods](#).

Animals. Experiments were conducted according to protocols approved by the Animal Care and Use Committee of the Institute of Molecular Genetics, Czech Academy of Sciences. All experiments were performed with littermates (males and females) cross-bred from two transgenic mouse lines: floxed *Hif1a*^{tm3Rsj0} with exon 2 of the *Hif1a* gene flanked by loxP sites (*Hif1a*^{loxP/loxP}) (17) and *Isl1-Cre* (*Isl1*^{tm1(cre)SevJ+}) (24). *Hif1a*^{+/-loxP} or *Hif1a*^{loxP/loxP} mice served as controls. Control and heterozygous *Isl1-Cre;Hif1a*^{+/-loxP} mice were born and survived according to the expected Mendelian ratio of genotypes. To determine the efficiency of CRE-mediated recombination, *Isl1-Cre* mice were bred with *Rosa26* (*Gt(ROSA)26Sor*^{tm150r}) reporter mice. Phenotyping and data analysis were performed by investigators blinded to the genotypes of the mice.

Detection of *Hif1a* Exon 2 Deletion. DNA was isolated from embryonic hearts and forebrains at E10.5. Primers for exon 2 and exon 3 of the *Hif1a* gene were used for qPCR as described previously (67). The difference (Δ) between the quantification cycle (Cq) of exon 2 and Cq of exon 3 was determined for each sample, and Δ Cq values were compared between groups of *Hif1aCKO* and control mice using an unpaired two-tailed *t* test (GraphPad Prism 7). The relative amount of exon 2 DNA was calculated, based on the following formula: $\Delta\Delta$ Cq = Δ Cq of *Hif1aCKO* - Δ Cq of control (68).

Echocardiography. Echocardiographic evaluation of geometrical and functional LV parameters was performed using the GE Vivid 7 Dimension (GE Vingmed Ultrasound) with 12-MHz linear matrix probe M12L. The diastolic and systolic dimensions of the LV were measured in 12-wk-old mice as described previously (43).

Coronary Artery Visualization by Micro-CT Imaging. Hearts perfused with polymerized yellow Microfil (Flow Tech) were prepared as described previously (69) and processed by micro-CT scanning (SkyScan 1272; Bruker). Projection images were reconstructed using NRecon SW (Bruker). 3D visualizations were achieved with CTvox SW (Bruker). For some specimens, CTAnalyser SW (Bruker) was applied for removal of excess extravascular contrast that limited image clarity. Branching of coronary arteries was evaluated using 3D visualization, and distances between branches of the left coronary artery were measured in 3D.

Cranial Morphometry. Whole mouse cadavers were scanned on an Albira MikroPET/CT scanner (Bruker), and micro-CT images were used for measurement of the LCB skull dimension, the distance between the anterior point of premaxilla and occipital condyles. Skulls were reoriented in 3D using DataViewer SW (Bruker) to reach the same position for all specimens. Distances (LCB) were measured in the sagittal plane of 3D visualization.

Statistical Methods. Data are presented as mean \pm SEM. Differences between two groups were analyzed by an unpaired two-tailed *t* test. The Mann-Whitney *U* test was used when Gaussian distribution could not be assumed. Differences between groups were considered significant at $P < 0.05$. All statistical tests were performed using GraphPad Prism 7. Sample sizes and individual statistical results for all analyses are provided in the figure legends and tables.

ACKNOWLEDGMENTS. We thank the Imaging Methods Core Facility at Biotechnology and Biomedicine Centre of the Academy of Sciences and Charles University (BIOCEV) and micro-CT at the First Faculty of Medicine (CZ.1.05/41.00/16.0346). We also thank A. Pavlinek for manuscript editing and Nanduri Prabhakar (University of Chicago) for helpful discussions and presubmission manuscript review. This research was supported by Czech Science Foundation Grants 17-04719S and 19-07378S (to G.P.); institutional support of Czech Academy of Sciences Grant RVO 86652036 (to G.P.); European Regional Development Fund Grant BIOCEV CZ.1.05/1.1.00/02.0109 (to G.P.); and Czech Ministry of Education, Youth and Sports [Grants Progres Q29 (to M.B.) and Progres Q38 (to D.S.)], European Cooperation in Science and Technology (INTER-COST) Award LTC17023, and Czech Bio-Imaging Award LM20150621.

1. K. Kimura, M. Ieda, K. Fukuda, Development, maturation, and transdifferentiation of cardiac sympathetic nerves. *Circ. Res.* **110**, 325–336 (2012).
2. H. L. Leistner *et al.*, Heart rate and heart rate variability during sleep in aborted sudden infant death syndrome. *J. Pediatr.* **97**, 51–55 (1980).
3. M. Vaseghi, K. Shivkumar, The role of the autonomic nervous system in sudden cardiac death. *Prog. Cardiovasc. Dis.* **50**, 404–419 (2008).
4. H. Rohrer, Transcriptional control of differentiation and neurogenesis in autonomic ganglia. *Eur. J. Neurosci.* **34**, 1563–1573 (2011).
5. K. Huber, The sympathoadrenal cell lineage: Specification, diversification, and new perspectives. *Dev. Biol.* **298**, 335–343 (2006).
6. D. G. Gonsalvez *et al.*, Proliferation and cell cycle dynamics in the developing stellate ganglion. *J. Neurosci.* **33**, 5969–5979 (2013).
7. Y. Kameda, Signaling molecules and transcription factors involved in the development of the sympathetic nervous system, with special emphasis on the superior cervical ganglion. *Cell Tissue Res.* **357**, 527–548 (2014).
8. M. R. Potzner *et al.*, Sequential requirement of Sox4 and Sox11 during development of the sympathetic nervous system. *Development* **137**, 775–784 (2010).
9. K. Huber *et al.*, The LIM-homeodomain transcription factor Islet-1 is required for the development of sympathetic neurons and adrenal chromaffin cells. *Dev. Biol.* **380**, 286–298 (2013).
10. Q. Zhang *et al.*, Temporal requirements for ISL1 in sympathetic neuron proliferation, differentiation, and diversification. *Cell Death Dis.* **9**, 247 (2018).
11. T. Irie *et al.*, Cardiac sympathetic innervation via middle cervical and stellate ganglia and antiarrhythmic mechanism of bilateral stellectomy. *Am. J. Physiol. Heart Circ. Physiol.* **312**, H392–H405 (2017).
12. B. J. Pardini, D. D. Lund, P. G. Schmid, Organization of the sympathetic postganglionic innervation of the rat heart. *J. Auton. Nerv. Syst.* **28**, 193–201 (1989).
13. J. Nam *et al.*, Coronary veins determine the pattern of sympathetic innervation in the developing heart. *Development* **140**, 1475–1485 (2013).
14. H. Liu *et al.*, Role of VEGF and tissue hypoxia in patterning of neural and vascular cells recruited to the embryonic heart. *Dev. Dyn.* **238**, 2760–2769 (2009).
15. N. V. Iyer *et al.*, Cellular and developmental control of O₂ homeostasis by hypoxia-inducible factor 1 α . *Genes Dev.* **12**, 149–162 (1998).
16. V. Compennolle *et al.*, Cardia bifida, defective heart development and abnormal neural crest migration in embryos lacking hypoxia-inducible factor-1 α . *Cardiovasc. Res.* **60**, 569–579 (2003).
17. H. E. Ryan *et al.*, Hypoxia-inducible factor-1 α is a positive factor in solid tumor growth. *Cancer Res.* **60**, 4010–4015 (2000).
18. J. Krishnan *et al.*, Essential role of developmentally activated hypoxia-inducible factor 1 α for cardiac morphogenesis and function. *Circ. Res.* **103**, 1139–1146 (2008).
19. Y. Huang *et al.*, Cardiac myocyte-specific HIF-1 α deletion alters vascularization, energy availability, calcium flux, and contractility in the normoxic heart. *FASEB J.* **18**, 1138–1140 (2004).
20. N. Guimaraes-Camboa *et al.*, HIF-1 α represses cell stress pathways to allow proliferation of hypoxic fetal cardiomyocytes. *Dev. Cell* **33**, 507–521 (2015).
21. P. O. Schnell *et al.*, Regulation of tyrosine hydroxylase promoter activity by the von Hippel-Lindau tumor suppressor protein and hypoxia-inducible transcription factors. *J. Neurochem.* **85**, 483–491 (2003).
22. J. Milosevic *et al.*, Lack of hypoxia-inducible factor-1 alpha impairs midbrain neural precursor cells involving vascular endothelial growth factor signaling. *J. Neurosci.* **27**, 412–421 (2007).
23. C. L. Cai *et al.*, Isl1 identifies a cardiac progenitor population that proliferates prior to differentiation and contributes a majority of cells to the heart. *Dev. Cell* **5**, 877–889 (2003).
24. L. Yang *et al.*, Isl1Cre reveals a common Bmp pathway in heart and limb development. *Development* **133**, 1575–1585 (2006).
25. M. Dvorakova *et al.*, Incomplete and delayed Sox2 deletion defines residual ear neurosensory development and maintenance. *Sci. Rep.* **6**, 38253 (2016).
26. L. Lin *et al.*, β -catenin directly regulates Islet1 expression in cardiovascular progenitors and is required for multiple aspects of cardiogenesis. *Proc. Natl. Acad. Sci. U.S.A.* **104**, 9313–9318 (2007).
27. I. Kramer *et al.*, A role for Runx transcription factor signaling in dorsal root ganglion sensory neuron diversification. *Neuron* **49**, 379–393 (2006).
28. T. Peng *et al.*, Coordination of heart and lung co-development by a multipotent cardiopulmonary progenitor. *Nature* **500**, 589–592 (2013).
29. I. Macova *et al.*, Neurod1 is essential for the primary tonotopic organization and related auditory information processing in the midbrain. *J. Neurosci.* **39**, 984–1004 (2019).
30. S. Provot *et al.*, Hif-1 α regulates differentiation of limb bud mesenchyme and joint development. *J. Cell Biol.* **177**, 451–464 (2007).
31. M. E. Mendelsohn, R. H. Karas, Molecular and cellular basis of cardiovascular gender differences. *Science* **308**, 1583–1587 (2005).
32. N. O. Glebova, D. D. Ginty, Heterogeneous requirement of NGF for sympathetic target innervation in vivo. *J. Neurosci.* **24**, 743–751 (2004).
33. X. Liang *et al.*, Transcription factor ISL1 is essential for pacemaker development and function. *J. Clin. Invest.* **125**, 3256–3268 (2015).
34. X. Liang *et al.*, HCN4 dynamically marks the first heart field and conduction system precursors. *Circ. Res.* **113**, 399–407 (2013).
35. D. Sedmera *et al.*, Changes in myocardial composition and conduction properties in rat heart failure model induced by chronic volume overload. *Front. Physiol.* **7**, 367 (2016).
36. A. Tittarelli, B. Janji, K. Van Moer, M. Z. Noman, S. Chouaib, The selective degradation of synaptic connexin 43 protein by hypoxia-induced autophagy impairs natural killer cell-mediated tumor cell killing. *J. Biol. Chem.* **290**, 23670–23679 (2015).
37. J. M. Pérez-Pomares *et al.*, Congenital coronary artery anomalies: A bridge from embryology to anatomy and pathophysiology. A position statement of the Development, Anatomy, and Pathology ESC Working Group. *Cardiovasc. Res.* **109**, 204–216 (2016).
38. S. L. Pfaff, M. Mendelsohn, C. L. Stewart, T. Edlund, T. M. Jessell, Requirement for LIM homeobox gene Isl1 in motor neuron generation reveals a motor neuron-dependent step in interneuron differentiation. *Cell* **84**, 309–320 (1996).
39. J. C. Kasemeier-Kulesa, J. A. Morrison, F. Lefcort, P. M. Kulesa, TrkB/BDNF signalling patterns the sympathetic nervous system. *Nat. Commun.* **6**, 8281 (2015).
40. G. L. Semenza, Oxygen sensing, homeostasis, and disease. *N. Engl. J. Med.* **365**, 537–547 (2011).
41. G. L. Semenza, Hypoxia-inducible factors in physiology and medicine. *Cell* **148**, 399–408 (2012).
42. R. Cerychova, G. Pavlinkova, HIF-1, metabolism, and diabetes in the embryonic and adult heart. *Front. Endocrinol. (Lausanne)* **9**, 460 (2018).
43. R. Cerychova *et al.*, Adverse effects of *Hif1a* mutation and maternal diabetes on the offspring heart. *Cardiovasc. Diabetol.* **17**, 68 (2018).
44. R. Bohuslavova, L. Skvorova, D. Sedmera, G. L. Semenza, G. Pavlinkova, Increased susceptibility of HIF-1 α heterozygous-null mice to cardiovascular malformations associated with maternal diabetes. *J. Mol. Cell. Cardiol.* **60**, 129–141 (2013).
45. Y. Sun *et al.*, A central role for Islet1 in sensory neuron development linking sensory and spinal gene regulatory programs. *Nat. Neurosci.* **11**, 1283–1293 (2008).
46. X. Yuan *et al.*, Disruption of spatiotemporal hypoxic signaling causes congenital heart disease in mice. *J. Clin. Invest.* **127**, 2235–2248 (2017).
47. N. Francis *et al.*, NT-3, like NGF, is required for survival of sympathetic neurons, but not their precursors. *Dev. Biol.* **210**, 411–427 (1999).
48. A. Hassankhani *et al.*, Overexpression of NGF within the heart of transgenic mice causes hyperinnervation, cardiac enlargement, and hyperplasia of ectopic cells. *Dev. Biol.* **169**, 309–321 (1995).
49. R. Schulz *et al.*, Connexin 43 is an emerging therapeutic target in ischemia/reperfusion injury, cardioprotection and neuroprotection. *Pharmacol. Ther.* **153**, 90–106 (2015).
50. R. Deo, C. M. Albert, Epidemiology and genetics of sudden cardiac death. *Circulation* **125**, 620–637 (2012).
51. A. A. Waza, K. Andrabi, M. U. Hussain, Protein kinase C (PKC)-mediated interaction between connexin43 (Cx43) and K⁺(ATP) channel subunit (Kir6.1) in cardiomyocyte mitochondria: Implications in cytoprotection against hypoxia-induced cell apoptosis. *Cell. Signal.* **26**, 1909–1917 (2014).
52. Y. Sun *et al.*, Islet 1 is expressed in distinct cardiovascular lineages, including pacemaker and coronary vascular cells. *Dev. Biol.* **304**, 286–296 (2007).
53. K. Kobayashi *et al.*, Targeted disruption of the tyrosine hydroxylase locus results in severe catecholamine depletion and perinatal lethality in mice. *J. Biol. Chem.* **270**, 27235–27243 (1995).
54. G. Faxelius, K. Hågnevik, H. Lagercrantz, B. Lundell, L. Irestedt, Catecholamine surge and lung function after delivery. *Arch. Dis. Child.* **58**, 262–266 (1983).
55. P. J. Schwartz *et al.*, Prolongation of the QT interval and the sudden infant death syndrome. *N. Engl. J. Med.* **338**, 1709–1714 (1998).
56. C. Le Magueresse *et al.*, Subventricular zone-derived neuroblasts use vasculature as a scaffold to migrate radially to the cortex in neonatal mice. *Cereb. Cortex* **22**, 2285–2296 (2012).
57. P. Himmels *et al.*, Motor neurons control blood vessel patterning in the developing spinal cord. *Nat. Commun.* **8**, 14583 (2017).
58. J. Duran *et al.*, The *HIF1A* C85T single nucleotide polymorphism influences the number of branches of the human coronary tree. *Cardiology* **121**, 156–159 (2012).
59. J. Wikenheiser *et al.*, Altering HIF-1 α through 2,3,7,8-tetrachlorodibenzo-p-dioxin (TCDD) exposure affects coronary vessel development. *Cardiovasc. Toxicol.* **13**, 161–167 (2013).
60. F. Pistollato *et al.*, Hypoxia and HIF1 α repress the differentiative effects of BMPs in high-grade glioma. *Stem Cells* **27**, 7–17 (2009).
61. D. J. Manalo *et al.*, Transcriptional regulation of vascular endothelial cell responses to hypoxia by HIF-1. *Blood* **105**, 659–669 (2005).
62. C. Ruiz de Almodovar *et al.*, VEGF mediates commissural axon chemoattraction through its receptor Flk1. *Neuron* **70**, 966–978 (2011).
63. Y. S. Mukoyama, H. P. Gerber, N. Ferrara, C. Gu, D. J. Anderson, Peripheral nerve-derived VEGF promotes arterial differentiation via neuropilin 1-mediated positive feedback. *Development* **132**, 941–952 (2005).
64. B. Oosthuyse *et al.*, Deletion of the hypoxia-response element in the vascular endothelial growth factor promoter causes motor neuron degeneration. *Nat. Genet.* **28**, 131–138 (2001).
65. T. Bishop *et al.*, Abnormal sympathoadrenal development and systemic hypertension in PHD3^{-/-} mice. *Mol. Cell. Biol.* **28**, 3386–3400 (2008).
66. G. L. Semenza, N. R. Prabhakar, The role of hypoxia-inducible factors in carotid body (patho) physiology. *J. Physiol.* **596**, 2977–2983 (2018).
67. K. Sarkar *et al.*, Hypoxia-inducible factor 1 transcriptional activity in endothelial cells is required for acute phase cardioprotection induced by ischemic preconditioning. *Proc. Natl. Acad. Sci. U.S.A.* **109**, 10504–10509 (2012).
68. M. W. Pfaffl, A new mathematical model for relative quantification in real-time RT-PCR. *Nucleic Acids Res.* **29**, e45 (2001).
69. H. Kolesová, M. Bartoš, W. C. Hsieh, V. Olejníčková, D. Sedmera, Novel approaches to study coronary vasculature development in mice. *Dev. Dyn.* **247**, 1018–1027 (2018).